

A study of pendular liquid bridge between two equal solid spheres

James Q. Feng

OXCBO Research, Maple Grove, Minnesota, USA

E-mail: james.q.feng@gmail.com

Abstract

Pendular liquid bridges with concave meridian between two equal rigid spheres are mathematically studied emphasizing on some less analyzed facts in the literature. Discrepancies from numerical solution of the Young-Laplace equation are examined among typical simplifying approximations as well as a few curve-fitting formulas. The separation distance between spheres is shown to play an important role in pendular ring formation via capillary condensation for a given relative humidity as well as the strength of subsequent capillary forces. For most practical situations, the toroidal approximation could be reasonably accurate (especially with diminishing separation distance) and can provide valuable mathematical insights at least in a qualitative sense with its relatively simple analytical formulas. Using the elliptic meridional profile generally offers more accurate approximations, but with so complicated analytical formulas that it would limit its convenience for practical applications. With a few examples, the present study shows that curve-fitting formulas cannot be perfect and by their approximative nature would always leave rooms for improvements; therefore, care should be taken to avoid undesirable errors.

Keywords: Young-Laplace equation, pendular bridge, capillary condensation, capillary forces, mathematical approximation

1 Introduction

Everyday experience indicates that moist sand (as well as soils, powders, granular materials in general) can be easily shaped for building castles, while dry sand flows without much cohe-

sivity, yet when too wet the sand would become soggy. Early study of soil cohesion property has suggested the important contributions of capillary forces when wet [1, 2]. To enable quantified analysis, the “ideal soil” with uniform rigid spheres in regular packing was considered for understanding the moisture effects on soil mechanics. With an idealized model, it is shown that the presence of a small amount of liquid between two solid spheres would form a so-called pendular ring meniscus which can exert substantial capillary forces on the spheres. Even when these spheres are not in solid-solid contact, they could still be connected by a liquid bridge with the pendular ring. The capillary forces associated with such an axisymmetric meniscus of pendular liquid bridge have been a subject of serious investigation by numerous authors over a century [3]–[11], due to their relevance to many natural phenomena and practical processes. Quantitative calculations of the capillary forces due to a pendular ring meniscus can be important for understanding not only the adhesion-cohesion of powder particles, but also the behavior of insects, frogs, and geckos [12, 13], as well as sintering of ceramic and metallic particles [14, 15], even relevant to stiction of slider in magnetic memory hard discs [16].

The physical mechanism for forming liquid bridge may be described by the Kelvin equation which indicates that capillary condensation could occur onto a liquid surface with negative mean curvature even in a subsaturated vapor environment. Moreover, the excess pressure due to the mean curvature of liquid bridge surface is a significant contributor to the capillary adhesion force between particles. Therefore, efforts have been made to determine the geometric shape and associated value of mean curvature of a liquid bridge surface, as solution of the well-established Young-Laplace equation which can only be computed numerically [7, 8]. Studies with the toroidal approximation [3, 9, 10] considerably simplified the calculations, but have been found inaccurate for some situations [4, 5, 17]. In view of the inconvenience with numerical computations, Lian and Seville [18] started to develop analytical formulas by curve-fitting numerically computed results, for general usage. However, the curve-fitting approach could not

satisfy all the needs arising from various applications; hence similar efforts has been continuing to the present day [19, 20]. Recently, Kruyt and Millet [11] has suggested an interesting analytical model with elliptic approximation of the meniscus meridional profile, significantly improving the accuracy from the toroidal model but involving lengthy algebraic manipulations.

The present work would examine discrepancies among typical simplifying approximations as well as accuracy of a few curve-fitting formulas, emphasizing on mathematical explanations of some less analyzed aspects in the literature with a hope to provide enhanced understanding and confidence in calculated values.

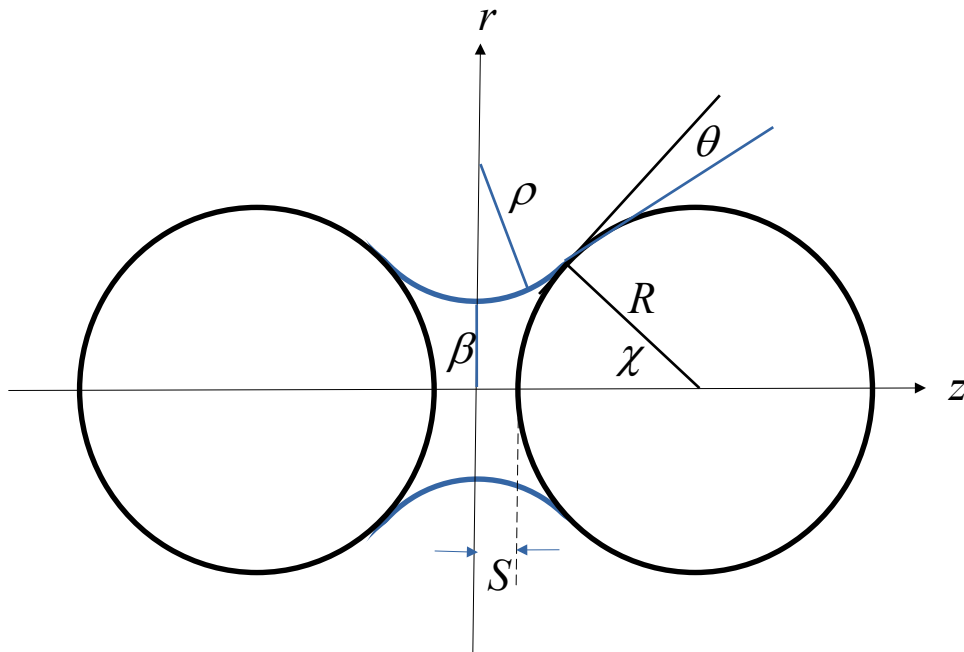


Figure 1: Illustrative sketch of a pendular liquid bridge between two equal solid spheres with a half separation distance S , the three-phase contact point at $z_c = S + R(1 - \cos \chi)$ and $r_c = R \sin \chi$, liquid-solid wetting angle θ and liquid half filling angle χ (where β denotes the bridge neck radius and r the radius of curvature of bridge meridional profile)

2 Problem Formulation

Considered here is a pendular liquid bridge with concave meridian formed between two equal solid spheres of radius R separated by a distance of $2S$, with the liquid-solid wetting angle θ and half-filling angle χ as depicted in figure 1 (based on the toroidal approximation). Motivated by the interest in water vapor assisted sintering of metal nanoparticle inks for printed electronics [21], the length scales in this study are assumed sufficiently small that the effect of gravity is negligible; hence, the pressure inside liquid has a constant value determined solely by the mean curvature of the axisymmetric meniscus and liquid surface tension σ . Therefore, the free surface shape of liquid bridge becomes the essential basis for subsequent analyses.

For presentation clarity with consistent nomenclature, most of the mathematical details are retained in the following subsections. To keep discussion well focused, the attention here is restricted to the situation of concave meridian, i.e., with $\chi + \theta \leq \pi/2$ and hence $\beta \leq r_c$.

2.1 Governing equations

The shape of axisymmetric free surface $r(z)$ is governed by the Young-Laplace equation [7, 8, 11]

$$2H = \nabla \cdot \mathbf{n} = \frac{1}{r\sqrt{1+(dr/dz)^2}} - \frac{d^2r/dz^2}{[1+(dr/dz)^2]^{3/2}} = \frac{\Delta p}{\sigma} \quad , \quad (1)$$

where the unit normal vector at liquid bridge surface is defined as

$$\mathbf{n} = \frac{\mathbf{e}_r - (dr/dz)\mathbf{e}_z}{\sqrt{1+(dr/dz)^2}} = \frac{(dz/dr)\mathbf{e}_r - \mathbf{e}_z}{\sqrt{1+(dz/dr)^2}} \quad , \quad (2)$$

and Δp denotes the excess pressure inside liquid bridge, σ the surface tension.

To complete the problem description, there are boundary conditions to be satisfied

$$\frac{dr}{dz} = 0 \quad \text{at } z = 0 \quad (\text{where } r = \beta) \quad ; \quad (3)$$

$$\frac{dr}{dz} = \tan\left(\frac{\pi}{2} - \chi - \theta\right) \quad \text{at } z_c = S + R(1 - \cos\chi) \quad (\text{and } r_c = R \sin\chi) \quad . \quad (4)$$

Thus, the mathematical problem becomes well-defined with the specified values of R , S , χ and θ , leaving β as a parameter to be determined as part of the solution. It can also be done by specifying R , β , χ and θ , but leaving S as a parameter to be determined as part of the solution [11], among other possibilities.

2.2 Solution to the Young-Laplace equation

Now, for a rigorous calculation, the Young-Laplace equation (1) can be rearranged as

$$2H = \nabla \cdot \mathbf{n} = \frac{dz/dr}{r\sqrt{1+(dz/dr)^2}} + \frac{d^2z/dr^2}{[1+(dz/dr)^2]^{3/2}} = \frac{\Delta p}{\sigma} \quad (5)$$

where

$$\frac{d^2z/dr^2}{[1+(dz/dr)^2]^{3/2}} = \frac{d}{dr} \left[\frac{dz/dr}{\sqrt{1+(dz/dr)^2}} \right] = \frac{du}{dr} \quad ,$$

with $u = \cos \varpi$ and ϖ being the angle between the tangent to the meridian curve and z-axis.

Thus, the Young-Laplace equation becomes

$$\frac{du}{dr} + \frac{u}{r} = 2H = \frac{\Delta p}{\sigma} \quad , \text{ namely, } r \frac{du}{dr} + u = 2Hr \quad . \quad (6)$$

The first integral of (6) yields

$$ru = Hr^2 + C \quad . \quad (7)$$

At $z_c = S + R(1 - \cos \chi)$ and $r_c = R \sin \chi$, we have $dz/dr = \tan(\chi + \theta)$ and $u = \sin(\chi + \theta)$ (where $\varpi = \pi/2 - \chi - \theta$), yielding

$$C = R \sin \chi [\sin(\chi + \theta) - HR \sin \chi] \quad .$$

And as $z \rightarrow 0$, $dz/dr \rightarrow \infty$, $u \rightarrow 1$ and $r \rightarrow \beta$, leading to

$$C = \beta - H\beta^2 \quad .$$

Therefore, either the value of mean curvature H can be determined from a specified neck radius β (as adopted in the present work) or β from a given H

$$H(\beta) = \frac{R \sin \chi \sin(\chi + \theta) - \beta}{(R \sin \chi + \beta)(R \sin \chi - \beta)} \quad , \quad (8a)$$

$$\beta(H) = \frac{1 - \sqrt{1 - 4HR \sin \chi [\sin(\chi + \theta) - HR \sin \chi]}}{2H} \quad . \quad (8b)$$

Now, without completely solving the problem, it is already clear from (8a) that negative H can be obtained when $\beta > R \sin \chi \sin(\chi + \theta)$ because $R \sin \chi = r_c > \beta$ for a free surface with concave meridian . As $\chi + \theta \rightarrow \pi/2$, we would have $\beta \rightarrow R \sin \chi$ and $2H \rightarrow 1/\beta$ with the meniscus shape approaching that of a cylinder. Then negative H can only occur when the value of $\chi + \theta$ is substantially smaller than $\pi/2$. Thus, there must exist some value of $\chi + \theta = \arcsin[\beta/(R \sin \chi)]$ in between 0 and $\pi/2$ for $H = 0$.

The free surface shape of liquid bridge can thus be determined based on (7) by integrating (as discussed in Kruyt and Millet [11])

$$\frac{dz}{dr} = \frac{Hr^2 + C}{\sqrt{r^2 - (Hr^2 + C)^2}} \quad \text{thus} \quad z(r) = z_c - \int_r^{r_c} \frac{Hr^2 + C}{\sqrt{r^2 - (Hr^2 + C)^2}} dr \quad . \quad (9)$$

A physically meaningful value of β and then $H(\beta)$ in (8a) can be determined iteratively via numerical computing to satisfy the boundary condition of $z(0) = 0$ at $r = \beta$, i.e.,

$$\int_{\beta}^{r_c} \frac{Hr^2 + C}{\sqrt{r^2 - (Hr^2 + C)^2}} dr = z_c = S + R(1 - \cos \chi) \quad . \quad (10)$$

With the value of β and thus $H(\beta)$ in (8a) being determined, the value of $\Delta p/\sigma = 2H$ from (1) enables calculating the capillary forces on each sphere in a normalized form as (attractive if positive, following Orr et al. [7], Lian et al. [8], Kruyt and Millet [11])

$$F = \frac{F_{cap}}{\pi \sigma R} = \frac{\beta}{R} \left[2 - \frac{\beta}{R} \left(\frac{R \Delta p}{\sigma} \right) \right] = \sin \chi \left[2 \sin(\chi + \theta) - \sin \chi \left(\frac{R \Delta p}{\sigma} \right) \right] \quad . \quad (11)$$

as well as the liquid bridge volume

$$V_{bridge} + \frac{2\pi R^3}{3} (1 - \cos \chi)^2 (2 + \cos \chi) = 2\pi \int_{\beta}^{r_c} \frac{r^2 (Hr^2 + C)}{\sqrt{r^2 - (Hr^2 + C)^2}} dr \quad ,$$

which leads to the normalized volume measured in units of the sphere volume

$$V = \frac{3V_{bridge}}{4\pi R^3} = \frac{3}{2} \int_{\beta}^{r_c} \frac{r^2(Hr^2 + C)}{\sqrt{r^2 - (Hr^2 + C)^2}} dr - \frac{(1 - \cos \chi)^2(2 + \cos \chi)}{2} . \quad (12)$$

where the last term comes from the spherical cap of polar angle χ .

It is noteworthy that (11) indicates that the capillary forces $F > 0$ is guaranteed even when the normalized excess pressure $R\Delta p/\sigma = 2HR = R/\beta > 0$ at its maximum which makes $F = \beta/R$. The capillary forces in (11) can be calculated either by considering a force balance at the neck of liquid bridge $z = 0$ (e.g., Lian et al. [8]) or at $z = z_c$ (e.g., Orr et al. [7]), both yielding the same result as long as (8a) holds, consistent with physical expectation.

2.3 Toroidal approximation

Over a century of study, there has not been general closed-form analytical solutions found to (1)-(4); the exact solution could only be computed numerically. Now, if the free surface meridional profile $r(z)$ is approximated as a part of the circle of constant radius ρ , i.e., with a toroidal free surface [3, 9, 10],

$$z^2 + (r - \beta - \rho)^2 = \rho^2 \quad \text{or} \quad r(z) = \beta + \rho - \sqrt{\rho^2 - z^2} , \quad (13)$$

β and ρ can be explicitly determined from boundary conditions (3) and (4) based on the geometry. Thus, we could have (as in Lian et al. [8])

$$\frac{\rho}{R} = \frac{1 - \cos \chi + S/R}{\cos(\chi + \theta)} \quad \text{and} \quad \frac{\beta}{R} = \sin \chi - \frac{\rho}{R}[1 - \sin(\chi + \theta)] , \quad (14)$$

which leads to the curvature terms in (1)

$$\frac{1}{r\sqrt{1 + (dr/dz)^2}} = \frac{1 - (z/\rho)^2}{r} \quad \text{and} \quad \frac{d^2r/dz^2}{[1 + (dr/dz)^2]^{3/2}} = \frac{1}{\rho} .$$

At $z = 0$, $dr/dz = 0$ and $r = \beta$ we get

$$\frac{1}{r\sqrt{1 + (dr/dz)^2}} = \frac{1 - (z/\rho)^2}{r} = \frac{1}{\beta} .$$

But at the contact circle $z = z_c = S + R(1 - \cos \chi)$ and $r = r_c = R \sin \chi$ we get

$$\frac{z_c}{\rho} = \cos(\chi + \theta), \quad \frac{1}{r\sqrt{1 + (dr/dz)^2}} = \frac{1 - (z/\rho)^2}{r} = \frac{\sin(\chi + \theta)}{R \sin \chi} \leq \frac{1}{\beta},$$

because $R \sin \chi \geq \beta$ and $\sin(\chi + \theta) \leq 1$.

As pointed out by Lian et al. [8], the toroidal free surface does not have a constant mean curvature H in the Young-Laplace equation (1); rather, its free surface shape corresponds to a variable mean curvature

$$\tilde{H}_c = \frac{1}{2} \left[\frac{\sin(\chi + \theta)}{R \sin \chi} - \frac{1}{\rho} \right] \leq \tilde{H} = \frac{\sqrt{1 - (z/\rho)^2}}{r} - \frac{1}{\rho} \leq \tilde{H}_0 = \frac{1}{2} \left(\frac{1}{\beta} - \frac{1}{\rho} \right). \quad (15)$$

It may then be natural to take an average

$$\tilde{H}_a = \frac{\tilde{H}_0 + \tilde{H}_c}{2} = \frac{3\beta R \sin \chi [\sin(\chi + \theta) - 1] + (R \sin \chi)^2 - \beta^2 \sin(\chi + \theta)}{4\beta R \sin \chi (R \sin \chi - \beta)}, \quad (16)$$

for approximating the actual H . But when it comes to calculating the capillary forces of (11), with the toroidal approximation, Lian et al. [8] considered two formulas based on either the local force balance at the neck of liquid bridge $z = 0$ with \tilde{H}_0 (as in Fisher [3]) or at the contact circle $z = z_c$ with \tilde{H}_c (as in Orr et al. [7]). However, the calculated value of differs depending on which formula is used. In fact, as shown in (11), the two formulas can yield the same result only when $\tilde{H}(\beta)$ is calculated via (8a). Therefore,

$$\tilde{F} = 2\beta(1 - \beta\tilde{H}_\beta)/R = 2 \sin \chi [\sin(\chi + \theta) - R \sin \chi \tilde{H}_\beta], \quad (17)$$

is used here for calculating the capillary forces, with $\tilde{H}_\beta(\beta)$ according to (8a) using the β determined from (14) for the toroidal approximation.

With the toroidal approximation, the normalized liquid bridge volume of (12) can now be explicitly written as

$$\begin{aligned} \tilde{V} = & \frac{3}{2} \left(\frac{\rho}{R} \right) \left[2 \left(\frac{\rho}{R} \right)^2 + 2 \frac{\rho}{R} \frac{\beta}{R} + \left(\frac{\beta}{R} \right)^2 \right] \cos(\chi + \theta) - \frac{1}{2} \left[\frac{\rho \cos(\chi + \theta)}{R} \right]^3 - \\ & - \frac{3}{2} \left(\frac{\rho}{R} \right)^2 \left(\frac{\rho}{R} + \frac{\beta}{R} \right) \left[\cos(\chi + \theta) \sin(\chi + \theta) + \frac{\pi}{2} - (\chi + \theta) \right] - \\ & - \frac{(1 - \cos \chi)^2 (2 + \cos \chi)}{2} \end{aligned}, \quad (18)$$

for straightforward calculations.

2.4 Elliptic meridional profile

To improve the analytical approximation, an elliptic meridional profile has been developed by Kruyt and Millet [11] as

$$\frac{z^2}{a^2} + \frac{(r-m)^2}{b^2} = 1 \quad \text{or} \quad r(z) = m - \frac{b}{a} \sqrt{a^2 - z^2} \quad , \quad (19)$$

where, based on the boundary conditions (3) and (4),

$$\begin{aligned} m &= \frac{z_c r_c - (r_c + \beta)(r_c - \beta) \tan(\chi + \theta)}{z_c - 2(r_c - \beta) \tan(\chi + \theta)} \\ b &= m - \beta \\ a &= \frac{z_c(m - \beta)}{\sqrt{(m - \beta)^2 - (m - r_c)^2}} \end{aligned} \quad . \quad (20)$$

For a given half-filling angle χ , the values of z_c and r_c are known. When the wetting angle θ is also specified, the neck radius β is still an adjustable parameter for determining the values of a , b , m in (19).

The elliptic meridional profile described by (19) leads to

$$\frac{dr}{dz} = \left(\frac{b}{a} \right) \frac{z}{\sqrt{a^2 - z^2}} \quad , \quad \frac{d^2r}{dz^2} = \frac{ab}{(a^2 - z^2)^{3/2}} \quad ,$$

and thus,

$$2\tilde{H}_e = \frac{[a^2 + b^2 + (b^2 - a^2)z^2/a^2]\sqrt{a^2 - z^2} - abm}{[m - (b/a)\sqrt{a^2 - z^2}][a^2 + (b^2 - a^2)z^2/a^2]^{3/2}} \quad . \quad (21)$$

The closure can be brought with a requirement of the value of β (which determines a , b , m) to have the same mean curvature value \tilde{H}_e at $z = 0$ and $z = z_c$ [11], namely

$$\frac{a^2 + b^2 - b m}{a^2(m - b)} = \frac{[a^2 + b^2 + (b^2 - a^2)z_c^2/a^2]\sqrt{a^2 - z_c^2} - abm}{[m - (b/a)\sqrt{a^2 - z_c^2}][a^2 + (b^2 - a^2)z_c^2/a^2]^{3/2}} \quad . \quad (22)$$

Unfortunately, (22) is an algebraically rather complicated equation for root-finding analytically in terms of β ; however, it can be computed with numerical iterations.

3 Results and Discussion

For presentation generality, the data shown here are computed by specifying $R = 1$ and $\sigma = 1$ which means to effectively measure length in units of R and excess pressure in units of σ/R . Hence, the values of S , H , etc. given here are the same as S/R , HR , etc. and used interchangeably.

3.1 Case of perfect wetting ($\theta = 0$)

With perfect wetting liquids, the wetting angle $\theta = 0$ and the capillary effects are expected to become maximized. Some authors (e.g., Erle et al. [22]) would only focus on computing the case of $\theta = 0$. So, it is worthwhile to take a close look at this special case.

3.1.1 Discrepancies among different approximations

Figure 2 shows the meridional profiles computed based on the Young-Laplace equation and approximations with toroidal meniscus and elliptic meridional profile, for the half filling angle $\chi = 15^\circ$ (and $\theta = 0$) at $S/R = 0$ ($V = 0.001197$) and 0.05 ($V = 0.003675$). It reveals the fact that the toroidal approximation can be quite reasonable when the separation distance S is small, with increasing S the discrepancies become more obvious although the elliptic approximation still remains close to the Young-Laplace solution.

For a constant liquid bridge volume $V = 0.001$, figure 3 shows the meridional profiles at $S/R = 0.06$ ($\chi = 9.615^\circ$) and 0.07 ($\chi = 10.33993^\circ$), indicating that the elliptic approximation may also deviate from the Young-Laplace solution in some circumstances.

According the empirical formula by Lian et al. [8] for determining the bridge rupture distance S_c (in the present nomenclature, with θ in radian)

$$\frac{S_c(V)}{R} = \frac{2 + \theta}{4} \left(\frac{4\pi V}{3} \right)^{1/3}, \quad (23)$$

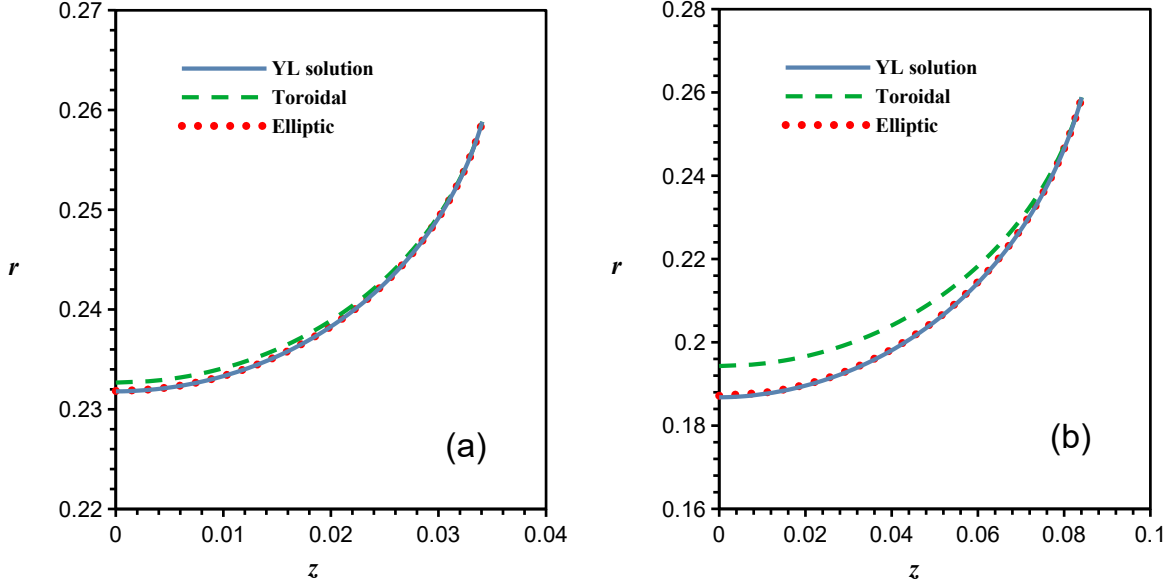


Figure 2: Comparison of meniscus meridional profiles computed based on solution of the Young-Laplace equation (9), toroidal approximation (13), and elliptic approximation (19), for $\chi = 15^\circ$ and $\theta = 0$ with (a) $S/R = 0$ and (b) $S/R = 0.05$

we would have $S_c/R = 0.0806$ and 0.1015 for $V = 0.001$ and 0.002 , which reveals a circumstance for the elliptic approximation to become inaccurate when $S/R (= 0.07$ for $V = 0.001$ as seen in figure 3, and 0.09 for $V = 0.002$ though not shown here, as indeed expected) is getting close to S_c/R . For a given liquid bridge volume V , solution for the Young-Laplace equation can only exist for $S \leq S_c$ whereat the solution branch encounters a turning point in the numerical computation [8], as also being verified with experiments [23].

To provide more concrete data for convenient comparison, table 1 shows computed values based on the Young-Laplace equation and those from the toroidal approximation (\tilde{H}_β in parentheses) for β/R , HR , and V at various specified S/R and χ (with $\theta = 0$). The comparison with the values from the Young-Laplace solutions reveals the fact that the toroidal model can be reasonably accurate when $\chi \rightarrow 0$ and $\chi \rightarrow \pi/2$, but becomes increasingly inaccurate when H

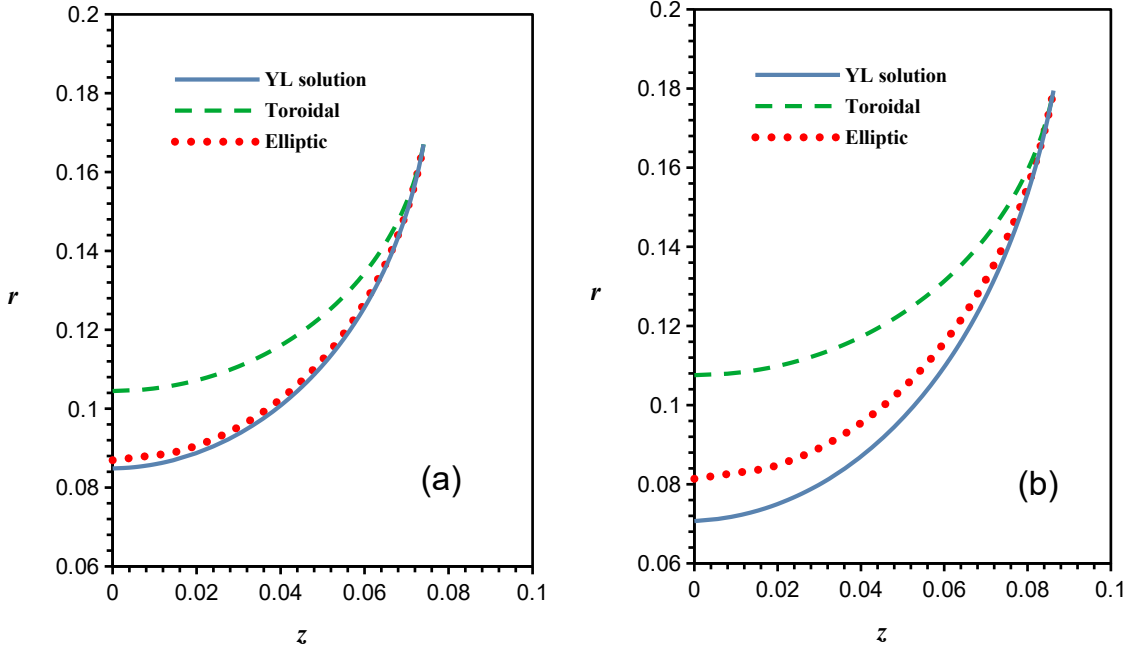


Figure 3: As figure 2 but for $V = 0.001$ according to (12) with (a) $S/R = 0.06$, $\chi = 9.615^\circ$, and (b) $S/R = 0.07$, $\chi = 10.33993^\circ$ (both at $\theta = 0$)

is approaching to zero, e.g., in the interval of $45^\circ < \chi < 60^\circ$ for $S/R = 0$. If the discrepancy of the toroidal \tilde{H}_β in parentheses from the Young-Laplace H becomes too large, it is natural to take a look at the toroidal \tilde{H}_a or \tilde{H}_0 as other available choices for approximation. For example, at $\chi = 45^\circ$ and $S/R = 0$ the value of \tilde{H}_a , \tilde{H}_0 would be -0.5303 , -0.3536 (while the value of \tilde{H}_e with the elliptic model is -0.4770 , much closer to the Young-Laplace $H = -0.4651$). If S/R is increased to 0.1 we would have $H = -0.1146$ but $\tilde{H}_a = -0.1906$, $\tilde{H}_0 = 0.01863$ with $\tilde{H}_\beta = -0.2178$, while $\tilde{H}_e = -0.1282$ (again much closer to H than the toroidal model). It appears that \tilde{H}_β and \tilde{H}_a are numerically rather close, differing from \tilde{H}_0 quite noticeably. If \tilde{H}_β and \tilde{H}_a are comparable in terms of accuracy, \tilde{H}_β might be preferred for consistency with the physical meaning of (17).

To illustrate varying mean curvature from $z = 0$ to z_c (here with length in units of R) with

Table 1: Comparison between computed values based on the Young-Laplace equation and those from the toroidal approximation (in parentheses) for β/R , HR , and V at various specified S/R and χ (with $\theta = 0$)

| S/R | χ (deg) | β/R | $HR(\tilde{H}_\beta R)$ | V |
|-------|--------------|-------------------|-------------------------|---|
| 0 | 5 | 0.08362 (0.08367) | -125.920 (-127.714) | 1.901×10^{-5} (1.905×10^{-5}) |
| | 15 | 0.2318 (0.2327) | -12.423 (-12.893) | 0.001197 (0.001212) |
| | 45 | 0.5775 (0.5858) | -0.4651 (-0.5469) | 0.05278 (0.05523) |
| | 60.63 | 0.7272 (0.7379) | 0.1397 (0.1002) | 0.1379 (0.1444) |
| | 89.9 | 0.99903 (0.99913) | 0.49946 (0.49934) | 0.49811 (0.49826) |
| 0.05 | 11.940 | 0.1403 (0.1488) | -4.2166 (-5.1323) | 0.002001 (0.002199) |
| 0.09 | 13.2511 | 0.08583 (0.1369) | -0.7369 (-2.4942) | 0.002000 (0.003553) |
| 0.1 | 15 | 0.1123 (0.1559) | -0.8339 (-2.0847) | 0.003347 (0.005140) |

the toroidal model and elliptic model, figure 4 provides two exemplifying cases: (a) $S = 0.1$ and $\chi = 45^\circ$ with the elliptic \tilde{H}_e being very close to the constant H than the toroidal \tilde{H} ; (b) $S = 0.09$ and $\chi = 13.2511^\circ$ with $V = 0.002$ wherewith even the elliptic \tilde{H}_e exhibits considerable deviations from the Young-Laplace solution, whereas the value of toroidal \tilde{H}_0 appears as a relatively better approximation.

Compared with the toroidal model, the elliptic model of Kruyt and Millet [11] indeed generally follows more closely with the Young-Laplace solution for $S/R = 0$ and $\chi < 60.631^\circ$. For example, at $\chi = 60.63^\circ$ the values of β/R , HR , and V from the elliptic model are 0.7281, 0.1345, and 0.1382 certainly much better than those of the toroidal model in table 1. However, when χ is increased beyond 60.631° there does not seem to exist a value of β/R that could satisfy the closure relationship (22).

With the elliptic approximation (19) there actually exists a few mathematical restrictions when examine the expression (20) for $a > 0$, $b > 0$, and $m > 0$ with $r_c > \beta$ to be physically meaningful. It seems to require that

$$z_c - 2(r_c - \beta) \tan(\chi + \theta) > 0 \quad \text{or} \quad r_c - \frac{z_c}{2 \tan(\chi + \theta)} < \beta < r_c \quad (24)$$

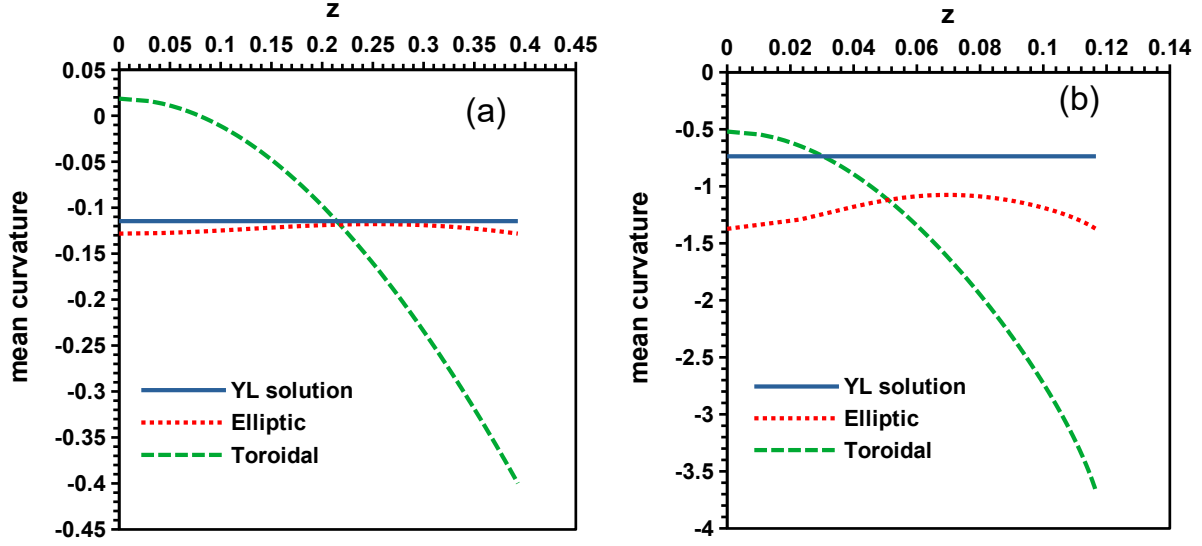


Figure 4: Varying mean curvature from $z = 0$ to z_c (in units of R) according to (15) for \tilde{H} of toroidal model and (21) of elliptic model for (a) $S/R = 0.1$, $\chi = 45^\circ$ with $\tilde{H}_\beta R = -0.2178$ at $z \sim 0.29$, and (b) $S/R = 0.09$, $\chi = 13.2511^\circ$ with $V = 0.002$, $\tilde{H}_\beta R = -1.8192$ at $z \sim 0.076$ (both at $\theta = 0$)

to guarantee $m > 0$ which actually leads to $m > r_c$ as a consequence. Clearly, $\chi + \theta$ could not exceed a value below $\pi/2$ due to (24). For example, at $S = 0$ and $\chi = 60.63^\circ$ the lower bound for β according to (24) would be 0.7280874, while at $\beta \sim 0.728087821$ the values of \tilde{H}_e from (21) at $z = 0$ and $z = z_c$ could match at ~ 0.1345025 . But when χ is increased to 60.631° , even when β approaches its lower bound value 0.728097533 the values of \tilde{H}_e at $z = 0$ and $z = z_c$ would still be ~ 0.134529 and ~ 0.134522 , could not match exactly. Hence, not all the values of β that satisfies (24) can also satisfy (22) for the mathematical closure.

It is interesting to note that with the toroidal approximation (14) is equivalent to

$$\beta = r_c - z_c \frac{1 - \sin(\chi + \theta)}{\cos(\chi + \theta)} \left(> r_c - \frac{z_c}{2 \tan(\chi + \theta)} \right) ;$$

thus, the condition (24) indicates that the lower bound of elliptic neck radius should always be

smaller than the toroidal β . As illustrated in figures 2 and 3, the toroidal neck radius appears always greater than the elliptic one that in turn (often just slightly) greater than that of the Young-Laplace solution.

3.1.2 Mean curvature and capillary condensation

The phenomenon of capillary condensation is usually rendered as vapor condensation that occurs at a concave vapor-liquid interface below the saturation vapor pressure of the pure liquid. To evaluate the mean curvature effect on vapor condensation for pendular liquid bridge formation, let's consider the Kelvin equation

$$\frac{p_v}{p_0} = \exp\left(\frac{2H\sigma M_w}{\rho_l N_A k_B T}\right), \text{ namely, } h = \exp(2H\lambda_K) \text{ or } 2HR = \frac{R \ln h}{\lambda_K}, \quad (25)$$

where p_v and p_0 denote the equilibrium vapor pressure at curved liquid surface and saturation vapor pressure at liquid surface of zero curvature (namely, flat liquid surface), M_w ($= 18.015 \times 10^{-3} \text{ kg mol}^{-1}$ for water) and ρ_l ($\sim 1000 \text{ kg m}^{-3}$ for water) the molecular weight (or molecular mass) and density of the bulk liquid, N_A and k_B the Avogadro's number and Boltzmann's constant ($N_A \times k_B = 8.3143 \text{ J deg}^{-1} \text{ mol}^{-1}$ is the so-called universal gas constant), and T the absolute temperature. Also in (25) $h = p_v/p_0$ denotes the "relative humidity" and $\lambda_K = \sigma M_w / (\rho_l N_A k_B T)$ the so-called Kelvin length [17].

Figure 5 illustrates how the excess pressure—related to twice the normalized mean curvature, i.e., $2HR$ —varies with half filling angle χ in radians, along with discrepancies of the toroidal model with \tilde{H}_β in (a) and \tilde{H}_0 in (b) in comparison with H computed from the Young-Laplace equation. Both \tilde{H}_β and \tilde{H}_0 deviate H noticeably when $\chi < \pi/4$, with \tilde{H}_0 overestimating while \tilde{H}_β underestimating the magnitude of negative H . However, both \tilde{H}_β and \tilde{H}_0 exhibit similar qualitative characteristics to that of $H(\chi)$: monotonic without minimum when $S = 0$ and having a minimum at a nonzero $\chi = \chi_{peak}$ when $S > 0$. Such characteristics may

be understood mathematically by taking advantage of the available analytical formulas with the toroidal approximation.

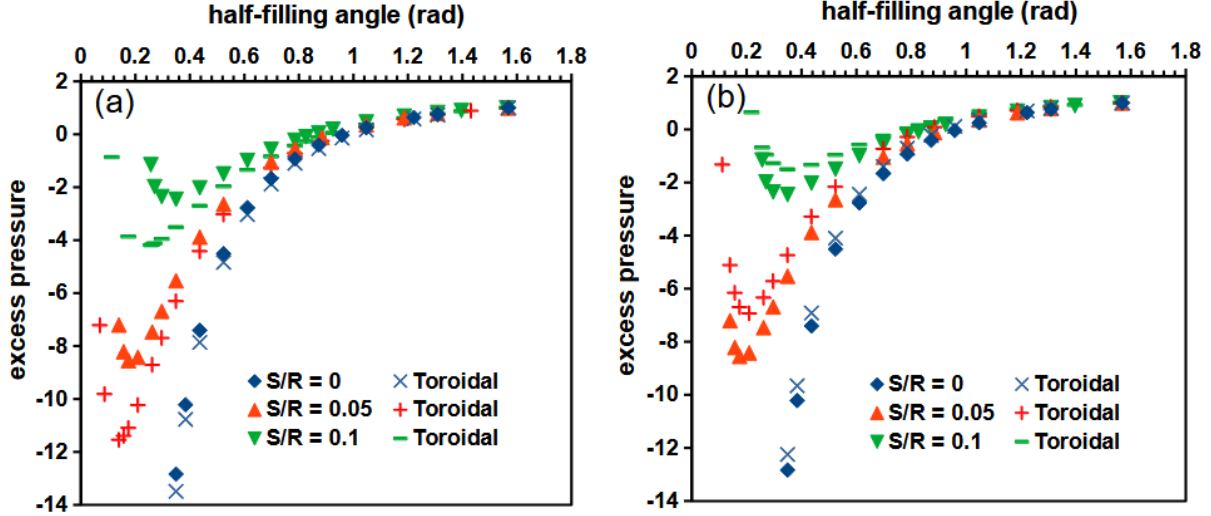


Figure 5: Computed excess pressure $R\Delta p/\sigma (= 2HR)$ in liquid bridge versus the half filling angle $\chi (< \pi/2)$ for various S/R , with comparison to the toroidal model based on (a) \tilde{H}_β and (b) \tilde{H}_0

In fact, having a minimum corresponds to the existence of two roots for $\tilde{H}_0 = 0$, which can easily be shown with the available analytical formulas (14) because $\tilde{H}_0 = 0$ is equivalent to

$$(1 + S/R)[2 - \sin(\chi + \theta)] - \cos \chi + \sin \theta = 0 \quad ,$$

namely,

$$\begin{aligned} & [(1 + S/R)^2 + 4 + 4(1 + S/R) \sin \theta] \sin^2 \chi - \\ & - 2[2(1 + S/R) + \sin \theta](1 + S/R) \cos \theta \sin \chi + \\ & + (S/R)(2 + S/R)(4 - \sin^2 \theta) = 0 \end{aligned}$$

which would generally have two distinct roots. But at $S = 0$, we encounter a ‘‘cusp’’ singularity

where the two roots degenerate to a single root

$$\sin \chi = \frac{2(2 - \sin \theta) \cos \theta}{5 + 4 \sin \theta} .$$

And for $\theta = 0$, the degenerated root becomes $\sin \chi = 4/5 = 0.8$ (at $S = 0$).

Viewed from another angle, the formulas in (14) indicate that $d\rho/d\chi > 0$ in the interval of $0 < \chi < \pi/2$ with minimum $\rho \propto S$ as $\chi \rightarrow 0$ (namely, $\rho \rightarrow 0$ can only happen when $S = 0$), while β can diminish at nonzero χ where ρ is definitely nonzero unless $S = 0$. Therefore, $\tilde{H}_0 = 1/\beta - 1/\rho$ would turn upward with reducing χ as long as $S \neq 0$.

Thus, the excess pressure curves of $2HR$ versus χ would have negative peaks, or minimum values, depending on the value of S/R , except the case for $S = 0$ to decrease indefinitely with diminishing χ . Such minimum values of $2HR$ correspond to the minimum “relative humidity” h for capillary condensation to occur at given values of S/R as can be calculated according to (25). A list of computed data with respect to water are provided in table 2 for $R = 25$ nm (corresponding to 50 nm diameter nanoparticles) at $T = 358.15K$ (i.e., 85°C) as a relevant situation for water-vapor assisted sintering of silver nanoparticle inks in printed electronics (cf. Bourassa et al. [21]). Hence at 85°C and 85% RH—a typical condition in a humidity chamber for environmental test of printed electronics robustness—one would expect water vapor condensation to happen when $2HR < -10$ with the mean radius of curvature $1/|2H| < 0.1R = 2.5$ nm in any $2S < 2.5$ nm, possibly approaching the applicability limit of the Kelvin equation [24].

If the particle size is increased to $R \sim 1 \mu\text{m}$, as those in the silty clay soil, for capillary condensation to occur at 0.95, 0.85, 0.75 RH and ambient temperature (e.g., 25°C) the value of $2HR$ would need to be $\sim -43.79, -138.74, -245.60$ corresponding to the mean radius of curvature $1/|2H| \sim 23, 7, 4$ nm in a very small gap between particles (i.e., with $S < 13, 6, 4$ nm). Apparently, the length scale for significant capillary condensation of water in clay soil is

Table 2: Computed values of β/R , F , V and h corresponding to $\chi = \chi_{peak}$ for the negative peak of excess pressure $2HR$ at various specified S/R for $R = 25$ nm and $T = 358.15^\circ\text{K}$ (with $\theta = 0$)

| S/R | χ_{peak} (deg) | $2HR$ | β/R | F | V | h |
|-------|---------------------|-----------|-----------|----------|------------------------|----------------------|
| 0.001 | 0.6 | -861.348 | 0.009387 | 0.094673 | 1.421×10^{-7} | 4.6×10^{-7} |
| 0.002 | 0.95 | -411.927 | 0.01437 | 0.11379 | 6.797×10^{-7} | 9.3×10^{-5} |
| 0.005 | 1.85 | -151.402 | 0.02656 | 0.15987 | 6.019×10^{-6} | 0.0769 |
| 0.01 | 3.1 | -68.8228 | 0.04222 | 0.20712 | 3.160×10^{-5} | 0.312 |
| 0.02 | 5.1 | -29.8976 | 0.06427 | 0.25206 | 0.0001541 | 0.603 |
| 0.05 | 10.5 | -8.58884 | 0.1170 | 0.35165 | 0.001398 | 0.865 |
| 0.1 | 19 | -2.45908 | 0.1913 | 0.47264 | 0.008133 | 0.959 |
| 0.15 | 26.5 | -0.71226 | 0.2481 | 0.53999 | 0.02167 | 0.988 |
| 0.195 | 33.5 | -0.007148 | 0.3054 | 0.61145 | 0.04387 | 0.99988 |

on the order of a few nanometers, barely within the validity limit of capillary theory [25, 26] .

Noteworthy here from table 2 is the fact that capillary forces F corresponding to the peak excess pressure decreases with reducing S , while the potential for capillary condensation increases with lowering h , as long as S is nonzero. Only when $S = 0$ could F increase with lowering h for contacting spheres.

3.1.3 Capillary forces

Formation of pendular liquid bridge between spheres would induce capillary forces ($F_{cap} \propto \sigma R$ on each sphere) with subsequent capillary cohesive strength—forces across unit cross-sectional area—($\propto \sigma/R$ for various packing configurations of spheres) increasing as the size of spheres decreases. Therefore, evaluating the value of capillary forces F in (11) is of practical importance.

Figure 6 shows curves of normalized capillary forces F in (11) versus half filling angle χ for $S/R = 0, 0.05$, and 0.1 . Like that in figure 5, the curve of $S = 0$ is monotonic and apparently linear, quite different from those of nonzero S . In contrast, with a nonzero S the magnitude of F would sharply decrease with reducing χ (e.g., for $\chi < 50^\circ$). The comparison

between the toroidal values of \tilde{F} based on \tilde{H}_β and \tilde{H}_0 (at $z = 0$) indicates that \tilde{H}_β -based values over-estimates while \tilde{H}_0 -based ones generally under-estimates the capillary forces though as a relatively better approximation. In general, the toroidal approximation for capillary forces does not seem too bad in view of its mathematical convenience with rigorously derived closed-form formulas.

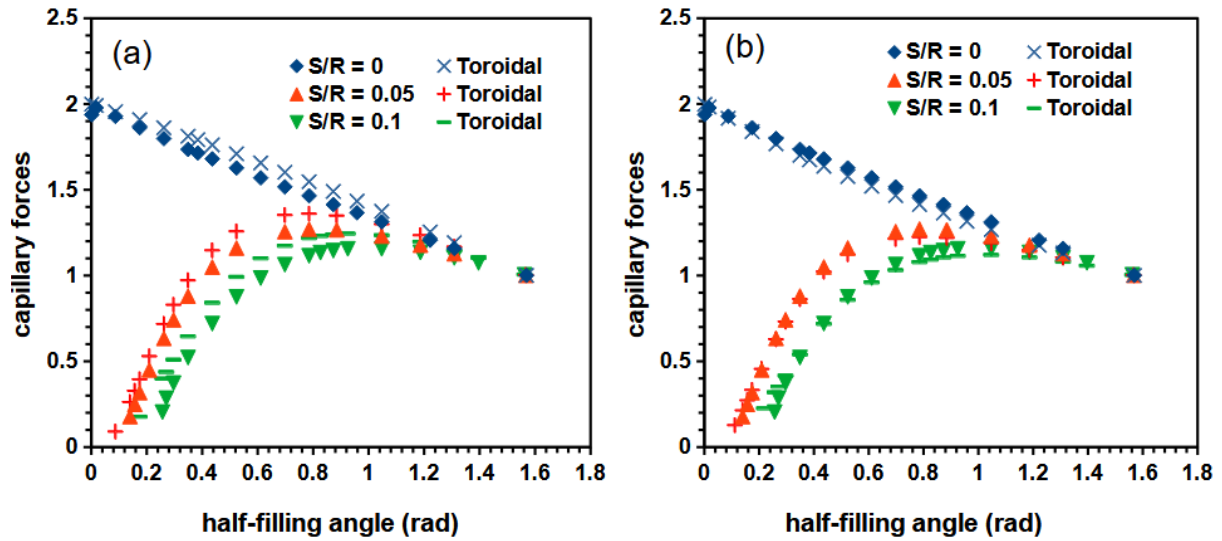


Figure 6: As figure 5 but for capillary forces F computed according to (11)

Corresponding to figure 5 with qualitative difference between the excess pressure $2HR$ curve of $S = 0$ and those with nonzero S , the curve of capillary force for $S = 0$ also exhibits different characteristics from those of nonzero S . With reducing χ the value of neck radius β would shrink and, as a consequence, F would be also expected to decrease with shrinking β in view of the expression in (11) for $z = 0$. Only when $S = 0$ would F approach a finite value as χ and β diminish where the value of $(1 - \beta HR)$ increases indefinitely (with $HR \rightarrow -\infty$). Thus, the case of $S = 0$ has its special place in studying the capillary effects of pendular liquid bridges.

As shown by Lian and Seville [18], the $S/R = 0$ curve can be fitted into a simple formula (in the present nomenclature)

$$F = 2 - 0.66\chi^{0.92} \quad , \quad (26)$$

which is quite accurate (for $\chi > 1^\circ$ with relative errors $< 0.8\%$). However, such an exceptional success might be just fortuitous. Several other curve-fitting formulas of Lian-Seville [18] do not seem as accurate as desirable under close examination.

3.1.4 Formulas based on curve-fitting

For convenient general usage, Lian and Seville [18] provides some “closed-form” formulas obtained by curve-fitting numerically computed results, among which there is an exceptionally simple relationship between (normalized) liquid bridge volume and half filling angle $\chi (< 60^\circ)$ for $\theta = 0$ and $S = 0$

$$V = 0.156131\chi^{3.73} \quad , \quad (27)$$

where $0.156131 = 0.654 \times 3/(4\pi)$ comes from the present definition of V in (12) which differs from that of Lian and Seville [18] by a factor of $(4\pi/3)$. However, (27) does not seem to be very accurate beyond $\chi = 45^\circ$ as shown in table 3. In contrast, the curve-fitting formulas in terms of polynomials (28) can be quite accurate for $\chi > 10^\circ$; interestingly, the analytical formula from toroidal model (18) seems to be quite accurate for calculating V for $\chi < 15^\circ$ (cf. Table 3).

$$V = 0.139205\chi^3 - 0.0259706\chi^2 + 0.0017335\chi \quad , \quad \text{for } 10^\circ < \chi < 65^\circ \quad (28a)$$

$$V = 0.064212\chi^4 - 0.054286\chi^3 + 0.18199\chi^2 - 0.0919611\chi + 0.014827 \quad , \quad \text{for } \chi > 60^\circ \quad (28b)$$

Another curved-fitting formula of Lian and Seville [18] is the liquid bridge neck radius as a monotonic function of half filling angle for $S = 0$ and $\theta = 0$, (29a), which does not seem very accurate with more than 10% relative errors for $\chi > \pi/3$ ($> 15\%$ as χ approaches $\pi/2$). Again, a much more accurate formula can be obtained by a polynomial curve fitting, such as

Table 3: Comparison among various curve-fitting formulas against computed values based on the Young-Laplace equation and those from the toroidal approximation (in parentheses) for V at various χ with $S = 0$ and $\theta = 0$

| χ (deg) | V | Eq. (27) | Eq. (28a) | Eq. (28b) |
|--------------|---|------------------------|------------------------|-----------|
| 5 | 1.901×10^{-5} (1.905×10^{-5}) | 1.749×10^{-5} | 4.614×10^{-5} | 0.008155 |
| 10 | 2.674×10^{-4} (2.691×10^{-4}) | 2.321×10^{-4} | 2.525×10^{-4} | 0.004091 |
| 15 | 0.001197 (0.001212) | 0.001053 | 0.001175 | 0.002553 |
| 30 | 0.01376 (0.01419) | 0.01397 | 0.01379 | 0.01360 |
| 45 | 0.05282 (0.05523) | 0.06341 | 0.05287 | 0.05299 |
| 60 | 0.1333 (0.1397) | 0.1854 | 0.1334 | 0.1330 |
| 75 | 0.2731 (0.2823) | 0.4263 | 0.2704 | 0.2731 |
| 89.9 | 0.49811 (0.49826) | 0.8379 | 0.4772 | 0.4981 |

(29b), with relative errors $< 1\%$ for $\chi > 10^\circ$ (1.65% at $\chi = 5^\circ$).

$$\beta(\chi)/R = 0.7634\chi^{0.9179}, \text{ for } \chi < 30^\circ \quad (29a)$$

$$\beta(\chi)/R = 0.1127\chi^3 - 0.3921\chi^2 + 0.97503\chi, \text{ for } \chi > 5^\circ \quad (29b)$$

Substituting their power-law fitted formulas for (29a) and (26) into (11) for $z = 0$, Lian and Seville [18] derived an approximate equation for the mean curvature (with $S = 0$ and $\theta = 0$), which is not very good outside the interval of $1^\circ < \chi < 45^\circ$. If the formula (26) for $F(\chi)$ is used with (11) for $z = z_c$, without involving $\beta(\chi)$, the obtained equation

$$2HR = 2 \left(1 - \frac{1 - 0.33\chi^{0.92}}{\sin^2 \chi} \right), \quad (30)$$

can be a much more accurate formula (with relative errors within a few percents for $0.1^\circ < \chi < 90^\circ$) for calculating the mean curvature and excess pressure.

3.2 Cases of nonzero contact angle θ

When the liquid is only partially wetting the solid spheres (i.e., $\theta \neq 0$, with $0 < \theta < \pi/2$), the range of valid half filling angle shrinks to $0 < \chi < (\pi/2 - \theta)$ for a liquid bridge with

concave meridian. As shown in figure 7, the qualitative behavior of normalized excess pressure ($= 2HR$) versus half filling angle χ for nonzero θ remains the same as that for $\theta = 0$. However, the magnitude of negative peak value as well as the deviation of toroidal \tilde{H}_β from H tends to decrease with increasing θ (in fact, the difference between the \tilde{H}_β curve and H curve for the case of $\theta = 75^\circ$ would diminish to an almost unidentifiable level in the plot).

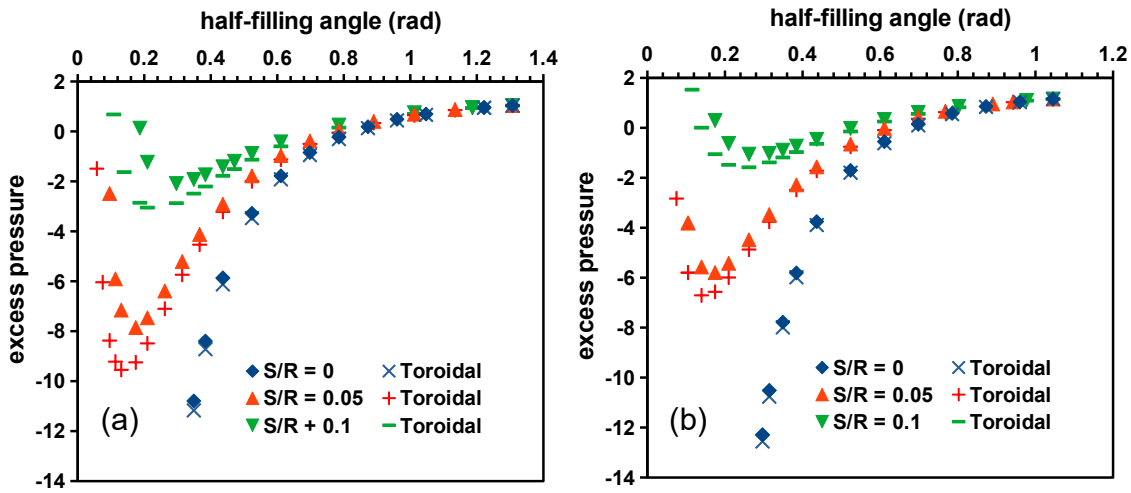


Figure 7: As figure 5 but for the cases of nonzero contact angle (a) $\theta = 15^\circ$ ($\chi < 75^\circ$) and (b) $\theta = 30^\circ$ ($\chi < 60^\circ$), with comparison to the toroidal model based on \tilde{H}_β

Again for $S = 0$, the magnitude of mean curvature can become indefinitely large with diminishing half filling angle which corresponds to diminishing liquid bridge volume, as indicated by degenerated single root for $H = 0$ discussed in subsection 3.1.2. Hence, a finite amount of liquid at a nonzero relative humidity would be expected to appear between two contacting spheres by virtue of capillary condensation. For a nonzero S whether a pendular liquid bridge can be maintained between two spheres depends on the value of S/R and relative humidity, similar to qualitative trends shown in table 2. The main effects of increasing θ is reducing the range of χ for liquid bridges with concave meridian to exist and the magnitude of peak

negative mean curvature for a given value of S/R .

Like the similarity of figures 5 and 7 for excess pressure, the curves of capillary forces for nonzero θ are quite similar to those in figure 6 too, and therefore unnecessary to be shown here.

4 Summary

With a systematic study along mathematical analysis, several less recognized behaviors of liquid bridges between spheres are revealed in the present work. Comparing with the Young-Laplace solution, the accuracy of toroidal as well as elliptic approximations is examined with mathematical explanations. At a given relative humidity, the separation distance between spheres appears to play an important role in pendular ring formation due to capillary condensation and the resulting magnitude of subsequent capillary forces.

With its relatively simple analytical formulas, the toroidal approximation can provide valuable mathematical insights at least in a qualitative sense and for most practical situations could be reasonably accurate (especially with diminishing separation distance). By a consideration for improved physical consistency, a new formula for calculating toroidal mean curvature is derived, differing from the commonly used formulas by previous authors. Although using the elliptic meridional profile generally offers improved approximations from the toroidal model, the complexity of its analytical formulas would limit the convenience for practical applications.

The present study also shows, with a few examples, that curve-fitting formulas cannot be perfect by their approximative nature and would always leave rooms for improvements. Therefore, care should be taken by checking their applicability conditions to avoid undesirable errors in serious applications.

Funding

None

Ethics declarations

Conflict of interests

The author has no conflicts to declare

References

- [1] Haines W B. A note on the cohesion developed by capillary forces in an ideal soil. *J. Agricultural Sci.* 15, 529-543 (1925)
- [2] Haines W B. Studies in the physical properties of soils. *J. Agricultural Sci.* 17, 264-299 (1927)
- [3] Fisher R A. On the capillary forces in an ideal soil; correction of formulae given by W. B. Haines. *J. Agricultural Sci.* 16, 492-505 (1926)
- [4] McFarlane J S, Tabor D. Adhesion of solids and the effect of surface films. *Proc. R. Soc. Lond. A* 202, 224-243 (1950)
- [5] Mason G and Clark W G. Liquid bridges between spheres. *Chem. Engng. Sci.* 20, 859-866 (1965)
- [6] Melrose J C. Model calculations for capillary condensation. *AIChE J.* 12(5), 986-994 (1966)
- [7] Orr F M, Scriven L E, Rivas A P. Pendular rings between solids: meniscus properties and capillary force. *J. Fluid Mech.* 67, 723-742 (1975)
- [8] Lian G, Thornton C, Adams M J. A theoretical study of the liquid bridge forces between two rigid spherical bodies. *Adv. Colloid Interface Sci.* 161, 138-147 (1993)

- [9] Megias-Alguacil D, Gauckler L J. Capillary forces between two solid spheres linked by a concave liquid bridge: regions of existence and forces mapping. *AIChE J.* 55, 1103-1109 (2009)
- [10] Megias-Alguacil D, Gauckler L J. Erratum to: Capillary and van der Waals forces between uncharged colloidal particles linked by a liquid bridge: regions. *Colloid Polym. Sci.* 288, 1501-1502 (2010)
- [11] Kruyt N P, Millet O. An analytical theory for the capillary bridge force between spheres. *J. Fluid Mech.* 812, 129-151 (2017)
- [12] Huber G, Mantz H, Spolenak R, Mecke K, Jacobs K, Gorb S N, Arzt E. Evidence for capillarity contributions to gecko adhesion from single spatula nanomechanical measurements. *Proc. Natl. Acad. Sci. USA* 102, 16293 (2005)
- [13] Qian J, Gao H. Scaling effects of wet adhesion in biological attachment systems. *Acta Biomater.* 2(1), 51-58 (2006)
- [14] Hwang K S, German R M, Lenel F V. Capillary forces between spheres during agglomeration and liquid phase sintering. *Metallurgical Transactions A* 18, 11-17 (1987)
- [15] Anestiev L A, Froyen L. Model of the primary rearrangement processes at liquid phase sintering and selective laser sintering due to biparticle interactions. *J. Appl. Phys.* 86(7), 4008-4017 (1999)
- [16] Mate C M. Application of disjoining and capillary pressure to liquid lubricant films in magnetic recording. *J. Appl. Phys.* 72, 3084-3090 (1992)
- [17] Butt H-J, Kappl M. Normal capillary forces. *Adv. Colloid Interf. Sci.* 146, 48-60 (2009)

- [18] Lian G, Seville J. The capillary bridge between two spheres: New closed-form equations in a two century old problem. *J. Colloid Interface Sci.* 227, 53-62 (2016)
- [19] Argilaga A, Zhao C. Rupture distances and capillary forces of liquid bridges: Closed-form expressions and ANNs-trained prediction models. *Powder Tech.* 427, 118702 (2023)
- [20] Bagheri M, Roy S, Poschel T. Approximate expressions for the capillary force and the surface area of a liquid bridge between identical spheres. *Computational Particle Mechanics* 11, 2179-2190 (2024) <https://doi.org/10.1007/s40571-024-00772-5>
- [21] Bourassa J, Ramm A, Feng J Q, Renn M J. Water vapor-assisted sintering of silver nanoparticle inks for printed electronics. *SN Applied Sciences* 1(6), 1-6 (2019)
- [22] Erle M A, Dyson D C, Morrow N R. Liquid bridges between cylinders, in a torus, and between spheres. *AIChE J.* 17, 115-121 (1971)
- [23] Willett C D, Adams M J, Johnson S A, Seville J P K. Capillary bridges between two spherical bodies. *Langmuir* 16, 9396-9405 (2000)
- [24] Fisher L R, Israelachvili J N. Experimental studies on the applicability of the Kelvin equation to highly curved concave menisci. *J. Colloid Interf. Sci.* 80(2), 528-541 (1981)
- [25] Giovambattista N, Almeida A B, Alencar A M, Buldyrev S V. Validation of capillarity theory at the nanometer scale by atomistic computer simulations of water droplets and bridges in contact with hydrophobic and hydrophilic surface. *J. Phys. Chem.* 120(3), 1597-1608 (2016)
- [26] Elliott J A W. Surface thermodynamics at the nanoscale. *J. Chem. Phys.* 154, 190901 (2021)